Environmental Science & Technology

Article

pubs.acs.org/est

Thermodynamic Controls on the Kinetics of Microbial Low-pH Fe(II) Oxidation

Lance N. Larson,[†] Javier Sánchez-España,[§] Bradley Kaley,[†] Yizhi Sheng,[†,‡] Kyle Bibby,[⊥] and William D. Burgos*[,†]

[†]Department of Civil and Environmental Engineering, The Pennsylvania State University, University Park, Pennsylvania 16802, United States

[§]Instituto Geológico y Minero de España (IGME), c/Calera 1, 28760 Tres Cantos, Spain

[‡]School of Water Resources and Environment, China University of Geosciences, Beijing 100083 China

[⊥]Department of Civil and Environmental Engineering, University of Pittsburgh, 709 Benedum Hall, Pittsburgh, Pennsylvania 15261, United States

Supporting Information

ABSTRACT: Acid mine drainage (AMD) is a major worldwide environmental threat to surface and groundwater quality. Microbial low-pH Fe(II) oxidation could be exploited for cost-effective AMD treatment; however, its use is limited because of uncertainties associated with its rate and ability to remove Fe from solution. We developed a thermodynamic-based framework to evaluate the kinetics of low-pH Fe(II) oxidation. We measured the kinetics of low-pH Fe(II) oxidation at five sites in the Appalachian Coal Basin in the US and three sites in the Iberian Pyrite Belt in Spain and found that the fastest rates of Fe(II) oxidation occurred at the sites with the lowest pH values. Thermodynamic calculations showed that the Gibbs free energy of Fe(II) oxidation ($\Delta G_{oxidation}$) was also most negative at the sites with the lowest pH values. We then conducted two series of microbial Fe(II) oxidation experiments in laboratory-scale chemostatic bioreactors operated through a series of pH values (2.1−4.2) and found the same relationships between Fe(II) oxidation kinetics, $\Delta G_{oxidation}$, and pH. Conditions that favored the fastest rates of Fe(II) oxidation coincided with higher Fe(III) solubility. The solubility of Fe(III) minerals, thus plays an important role on Fe(II) oxidation kinetics. Methods to incorporate microbial low-pH Fe(II) oxidation into active and passive AMD treatment systems are discussed in the context of these findings. This study presents a simplified model that describes the relationship between free energy and microbial kinetics and should be broadly applicable to many biogeochemical systems.

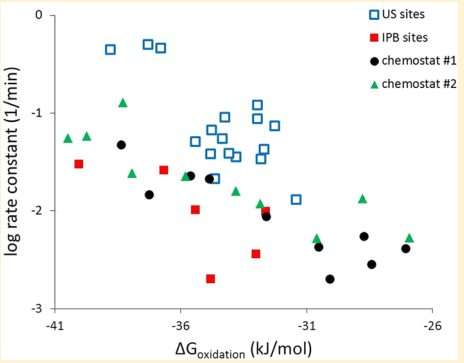

INTRODUCTION

Coal mine drainage (CMD) is the single largest cause of stream quality degradation in the Appalachian coal basins.[1] CMD can vary widely in its pH, acidity, and metal concentrations because of varied hydrogeochemical conditions. CMD sources also vary widely in their flow rates because of the relatively high, year-round rainfall in the Appalachian region and the presence of large underground mine pools. For example, in a study of 140 CMD sites (among thousands) in the Appalachian coal basins, Cravotta[2] reported that pH values ranged from 2.7 to 7.3, specific conductance ranged from 131 to 3,980 μS/cm, net acidity ranged from −326 to +1587 mg/L $CaCO_3$, total Fe ranged from 46 μg/L to 512 mg/L, and flow rate ranged from 0.028 to 2,210 L/s. Because of this great diversity in hydrogeochemical conditions, CMD remediation systems can be equally diverse in scale and biogeochemical processes employed for their treatment.

For acidic, Fe(II)-rich sources of CMD, microbial low-pH Fe(II) oxidation can be an effective component of an acid mine drainage (AMD) treatment system[3−5] At low-pH, abiotic Fe(II) oxidation by dissolved O_2 is slow. In contrast, the rate of microbial low-pH Fe(II) oxidation can be up to 5 orders of magnitude faster than abiotic oxidation.[6] However, the use of microbial low-pH Fe(II) oxidation for AMD treatment is limited because of uncertainties associated with its rate and ability to remove Fe from solution. For example, at a fixed pH of ∼pH 3.0, rates of Fe(II) oxidation have been reported to vary by more than 3 orders of magnitude.[7] The solubility of schwertmannite, the predominant mineral stable under these geochemical conditions,[8,9] is also highly variable with respect to stoichiometry and log K_{sp} as values have been reported from 5.8 to 39.5.[8−12] Uncertainties with respect to Fe(II) oxidation kinetics and Fe(III) solubility confounds treatment design and performance prediction.

Received: March 18, 2014
Revised: July 28, 2014
Accepted: July 29, 2014
Published: July 29, 2014

   dx.doi.org/10.1021/es501322d | Environ. Sci. Technol. 2014, 48, 9246−9254

We hypothesized that the products of Fe(II) oxidation, that is, soluble versus insoluble Fe(III), contribute to the wide range in reported rates of low-pH Fe(II) oxidation. At many AMD sites, microbial low-pH Fe(II) oxidation has led to the formation of terraced iron formations[3,13,14] (TIFs). In acidic, sulfate-rich waters, schwertmannite[8] (nominally $Fe_8O_8(SO_4)_{1.5}(OH)_5(s)$[9]) is commonly found as the predominant mineral across the surface of these TIFs.[13,14] The oxidation of Fe(II) occurs by

$$Fe^{2+} + \frac{1}{4}O_2 + H^+ = Fe^{3+}(aq) + \frac{1}{2}H_2O \quad (1)$$

While the precipitation of Fe(III) as schwertmannite occurs by

$$8Fe^{3+} + \frac{3}{2}SO_4^{2-} + 13H_2O = 21H^+ + Fe_8O_8(SO_4)_{1.5}(OH)_5 \quad (2)$$

Such that the oxidative precipitation of schwertmannite at low-pH occurs by

$$Fe^{2+} + \frac{1}{4}O_2 + \frac{3}{16}SO_4^{2-} + \frac{9}{8}H_2O = \frac{13}{8}H^+ + \frac{1}{8}Fe_8O_8(SO_4)_{1.5}(OH)_5(s) \quad (3)$$

Acidophilic microorganisms are responsible for catalyzing reaction 1, while geochemical conditions (e.g., dissolved concentrations of Fe^{3+} and SO_4^{2-}, pH, temperature) control the extent of reaction 2. Pesic et. al[15] and Kirby et. al[16] have proposed a rate formulation for reaction 1 similar to

$$R_{Fe(II)} = -\frac{d[Fe(II)]}{dt} = k \cdot C_{bact} \cdot [O_2] \cdot [Fe(II)] \cdot [H^+] \quad (4)$$

where $R_{Fe(II)}$ is the rate of Fe(II) oxidation (mol Fe(II) L^{-1} s^{-1}), k is the rate constant (L^3 mg^{-1} mol^{-2} s^{-1}), C_{bact} is the concentration of Fe(II)-oxidizing bacteria (mg L^{-1}, dry weight), $[O_2]$ is the dissolved or atmospheric equivalent concentration of oxygen (mol L^{-1}), and Fe(II) and H^+ are in mol L^{-1}. Importantly, this rate formulation predicts that the kinetics of microbial low-pH Fe(II) oxidation will increase proportionally with decreasing pH. Consistent with this prediction, Larson et. al[17] found that field rates of Fe(II) oxidation measured at multiple sites in the Appalachian Bituminous Coal Basin and the Iberian Pyrite Belt (IPB) were fastest at the sites with the lowest pH values.

In the current study, we have developed a thermodynamic-based framework to describe how the kinetics of microbial low-pH Fe(II) oxidation increases as pH decreases under field and controlled laboratory conditions. We conducted a series of laboratory experiments using two separate chemostatic bioreactors operated at a range of pH values (pH 2.1−4.2) to compare to field measurements. Results obtained from these laboratory experiments and from geochemically distinct regions (i.e., Appalachia versus IPB) were all consistent with thermodynamic calculations. An applied objective of this research is to translocate the biogeochemical processes occurring on natural TIFs into more space-efficient bioreactors for AMD treatment and optimize reactor conditions to maximize Fe(II) oxidation rates. Design modifications for active and passive systems for AMD treatment are proposed based on this analysis.

METHODS AND MATERIALS

Laboratory Fe(II) Oxidation Experiments. Mixed cultures of naturally occurring microbes were enriched from two different sites in central Pennsylvania for use in chemostatic (with respect to pH and temperature) bioreactor experiments. Chemostat 1 used sediments and water collected from Brubaker Run (40° 37′ 1.42″ N, 78° 28′ 35.76″ W), a field site that displayed an "average" rate of Fe(II) oxidation (Table 1). Chemostat 2 used sediments and water collected from Scalp Level (40° 14′43.72″ N, 78° 51′33.18″ W), a field site that displayed the fastest rate of Fe(II) oxidation among all sites in this study. Sediments were collected from the top 2−3 cm of each TIF, 30−45 m downstream of the emergent AMD sources. Emergent AMD was collected in large plastic containers, filtered (0.2-μm) after transportation to the laboratory, then containers were wrapped in aluminum foil and stored at 4 °C. One hundred grams of moist sediment was mixed with 1 L of 0.1% (m/v) sodium pyrophosphate (adjusted to pH 3.5 with sulfuric acid) for 30 min at 400 rpm. The suspension was then allowed to settle and 900 mL of the cell-containing supernatant was transferred into a sterile 3-L chemostat reactor vessel (Eppendorf BioFlo/Celligen 115 Fermentor). The reactor volume was increased to 2 L by adding filtered site water. The chemostat was then operated in a no-flow, fed-batch mode for 6 weeks. During this time the pH set-point was pH 2.9 for chemostat 1 or pH 2.7 for chemostat 2, the stirring rate was 50 rpm, and the temperature was 20 °C. The headspace of the reactor was open to the ambient atmosphere. Ferrous sulfate was discontinuously added to the reactor as the primary substrate to enrich for Fe(II)-oxidizing microbes. Ferrous sulfate was added to yield 300 mg L^{-1} dissolved [Fe(II)] and added whenever the dissolved [Fe(II)] decreased below 30 mg L^{-1}. After less than a month, the enrichment cultures required a daily dose of Fe(II). The fed-batch enrichment mode continued until the reactor consistently maintained an Fe(II) oxidation rate of 10−14 mg Fe(II) L^{-1} h^{-1}.

The reactors were then switched to flow-through mode (hydraulic residence time of 6 h). During all flow-through experiments, influent water was flushed with 100% N_2(g) and $FeSO_4$ was added to yield an average influent dissolved Fe(II) concentration of 300 mg/L. For chemostat 1, the pH set-point was varied by starting at pH 2.9 and sequentially adjusting to pH 2.6, 2.3, 2.6, 2.9, 3.2, 3.5, 3.8, 4.1, 3.8, and 3.5. For chemostat 2, the pH set-point was varied by starting at pH 2.7 and sequentially adjusting to pH 2.4, 2.1, 2.4, 2.7, 3.0, 3.3, 3.6, 3.9, and 4.2. Automatic feedback controls maintained the pH set-point by adding either 0.1 M H_2SO_4 or 0.2 M NaOH. For each pH set-point, the chemostat was operated until it had achieved a pseudosteady state condition with respect to maintaining a near-constant effluent dissolved Fe(II) concentration. The operating time for each pH set-point ranged from 20 to 50 pore volumes for chemostat 1, but was fixed at 50 pore volumes for chemostat 2.

Influent and effluent Fe was measured as total and dissolved based on 0.2-μm filtration. Fe(II) was measured using the ferrozine assay.[18] Total Fe, Fe(T), was measured using the ferrozine assay after reduction by 0.5 M hydroxylamine in 0.5 M hydrochloric acid. Biomass samples were collected at the end of the fed-batch enrichment mode and at the end of each pseudosteady state condition. Biomass was collected from a unit area of the reactor wall (1 cm^2) and a unit volume of the

dx.doi.org/10.1021/es501322d | Environ. Sci. Technol. 2014, 48, 9246−9254

Table 1. Geochemical Characteristics of the Emergent Waters from the Eight Field Sites and Corresponding Fe(II) Oxidation Kinetics[a]

	Appalachian Coal Basin, United States				Iberian Pyrite Belt, Spain			
	Brubaker Run	Scalp Level	Sulfur Run	Summerlee	Upper Red Eyes	La Zarza	Peña del Hierro	Rio Tintillo
latitude/longitude	40°37′1.42″N 78°28′35.76″W	40°14′43.72″N 78°51′33.18″W	40°18′25.91″N 78°44′5.06″W	38°0′18.06″N 81°9′29.04″W	40°14′27.07″N 78°44′25.42″W	37°42′22.70″N 6°51′48.38″W	37°43′30.41″N 6°33′21.62″W	37°42′31.86″N 6°37′14.06″W
temp (°C)	11.0 ± 0.26	13.3 ± 0.67	10.4 ± 0.15	14.6 ± 0.64	9.38 ± 0.46	26.5 ± 0.4	16.9 ± 2.1	24.3 ± 0.3
DO (mg/L)	0.06 ± 0.05	0.30 ± 0.06	0.14 ± 0.03	0.53 ± 0.6	0.18 ± 0.04	1.18 ± 0.8	2.75 ± 3.66	2.60 ± 3.1
ORP (mV)	348 ± 37	386 ± 39	315 ± 34	194 ± 49	284 ± 41	323 ± 14	423 ± 28	368 ± 8.5
specific conductance (μS/cm)	1,690 ± 236	2,010 ± 24	859 ± 41	1,890 ± 147	2,647 ± 44	7,440 ± 395	4,650	18,900 ± 117
pH	3.37 ± 0.15	2.89 ± 0.08	3.48 ± 0.07	4.32 ± 0.64	4.04 ± 0.03	3.13 ± 0.04	2.36 ± 0.12	2.96 ± 0.01
dissolved total Fe (mg/L)	118 ± 27.9	97.4 ± 9.43	105 ± 6.4	278 ± 57	395 ± 8.4	2,930 ± 294	1,220 ± 32	2,640 ± 151
dissolved Fe(II) (mg/L)	114 ± 28.4	92.3 ± 11.9	102 ± 6.5	275 ± 57	383 ± 20	2,740 ± 229	1,090 ± 61	2,310 ± 50
sulfate (mg S/L)	381 ± 89	429 ± 34	212 ± 44	547 ± 37	903 ± 100	2,530	1,180	8,190
acidity (mg/L $CaCO_3$)[b]	360	357	325	642	1,220	6,910	3,310	16,400
total PLFA (pmol/g)	25,200	6,500	20,100	18,700	20,200	n.d.	n.d.	n.d.
$R_{Fe(II),field}$ ($\times 10^7$ mol L^{-1} s^{-1})	16.0 ± 6.1	81.3 ± 39.0	21.6 ± 10.2	29.1 ± 17.0	14.3 ± 3.4	13.1 ± 9.40	67.9 ± 16.2	30.7 ± 1.10
$k_{Fe(II),field}$ (min^{-1})	0.070 ± 0.032	0.399 ± 0.132	0.066 ± 0.039	0.034 ± 0.015	0.038 ± 0.004	0.003 ± 0.001	0.028 ± 0.003	0.010 ± 0.003
n	5	3	3	3	3	2	2	2

[a]Values represent mean ± one standard deviation for n sampling events. n.d. = not determined [b]Acidity calculated according to Kirby and Cravotta [45]using mean metal concentrations.

reactor contents (135 mL) to measure attached and suspended biomass concentrations, respectively. A colorimetric protein assay (Bio-Rad) was used to measure biomass and calculated as cells mL^{-1} based on the manufacturer's conversion factor and geometric features of the reactor vessel. Biomass samples from chemostat 1 were also characterized by pyrosequencing. Details of these laboratory experiments are provided in the Supporting Information and in Kaley.[19]

Assuming that the chemostat operated as a completely mixed flow-through reactor at steady state, the rate of Fe(II) oxidation in the laboratory ($R_{Fe(II),lab}$; mol Fe(II) L^{-1} s^{-1}) was calculated as

$$R_{Fe(II),lab} = -\frac{d[Fe(II)]}{dt} = \frac{([Fe(II)_{in}] - [Fe(II)_{out}])}{\theta_h} \quad (5)$$

where $[Fe(II)_{in}]$ is the influent dissolved Fe(II) concentration, $[Fe(II)_{out}]$ is the effluent dissolved Fe(II) concentration, and Θ_h is the hydraulic residence of the reactor. Assuming that the rate of Fe(II) oxidation was dependent on the dissolved Fe(II) concentration, the first-order rate constant for Fe(II) oxidation in the laboratory ($k_{Fe(II),lab}$; min^{-1}) was calculated as

$$k_{Fe(II),lab} = \frac{([Fe(II)_{in}] - [Fe(II)_{out}])}{[Fe(II)_{out}] \cdot \theta_h} \quad (6)$$

Field Measurements of Fe(II) Oxidation Rates. Eight mine-impacted sites with natural TIFs were sampled (Table 1). Five sites were located in the Appalachian Bituminous Coal Basin of the United States and three sites were located in the Iberian Pyrite Belt (IPB) of southwestern Spain. These sites were selected to ensure a broad spectrum of geochemical and hydrological conditions for our thermodynamic calculations, and to compare rates of Fe(II) oxidation in Appalachian coal mine drainage versus IPB metal mine drainage. Sites in the US contained discharges associated with bituminous coal or clay mining that occurred in the mid to-late twentieth century. Sites in the IPB contained discharges associated with metal mining that occurred since pre-Roman times until present-day, and the ore deposits were composed of massive sulfides dominated by pyrite.[20]

For each site, geochemical profiles were established as longitudinal transects downstream from the emergent source using a combination of field measurements, water samples, and physical site characteristics, along a single flow path which conveyed the majority of the water across each TIF. Portable field meters were used to measure pH, oxidation−reduction potential (ORP), dissolved oxygen (DO), and temperature. Dissolved Fe(II) and dissolved total Fe(T) (after reduction by hydroxylamine-HCl) were determined using the ferrozine assay[18] with filtered (0.2-μm) samples preserved with HCl. Dissolved Fe(III) concentrations were determined from the difference of dissolved total Fe(T) and dissolved Fe(II) measurements. Rates of Fe(II) oxidation in the field were calculated using concentrations of dissolved Fe(II) versus travel time. Stream velocities were measured at each sampling location and used to transform concentration-versus-distance plots into concentration-versus-travel time. Water velocities were measured using a food color dye as a tracer along with a stopwatch and tape measure. Assuming that each stream reach functioned as a plug flow reactor with no other inputs of flow or dissolved Fe(II), the rate of Fe(II) oxidation in the field ($R_{Fe(II),field}$; mol Fe(II) L^{-1} s^{-1}) was calculated as

$$R_{\mathrm{Fe(II),field}} = -\frac{\mathrm{d[Fe(II)]}}{\mathrm{d}t} = \frac{([\mathrm{Fe(II)}_{\mathrm{inflow}}] - [\mathrm{Fe(II)}_{\mathrm{outflow}}])}{t} \quad (7)$$

where $[\mathrm{Fe(II)}_{\mathrm{inflow}}]$ is the dissolved Fe(II) concentration at the inflow to the TIF (i.e., emergent source of AMD), $[\mathrm{Fe(II)}_{\mathrm{outflow}}]$ is the dissolved Fe(II) concentration at the outflow from the TIF, and t is the travel time of the water from the inflow to the outflow of the TIF. Assuming that the rate of Fe(II) oxidation was dependent on the dissolved Fe(II) concentration, the first-order rate constant for Fe(II) oxidation in the field ($k_{\mathrm{Fe(II),field}}$; min^{-1}) was calculated as

$$k_{\mathrm{Fe(II),field}} = \frac{-\ln\left(\frac{[\mathrm{Fe(II)}_{\mathrm{outflow}}]}{[\mathrm{Fe(II)}_{\mathrm{inflow}}]}\right)}{t} \quad (8)$$

Phospholipid fatty acids (PLFAs) were used to measure biomass concentrations in the sediments at the five US field sites. PLFAs were analyzed for PLFA by Microbial Insights, Inc. (Rockford, TN, US). Details of these field measurements are provided in the Supporting Information and in Larson et. al.[17]

Thermodynamic Calculations. On the basis of reaction 1, the Gibbs free energy for Fe(II) oxidation ($\Delta G_{\mathrm{oxidation}}$) was calculated as

$$\Delta G_{\mathrm{oxidation}} = \Delta G^0_{\mathrm{oxidation}} + RT\cdot\ln\left(\frac{\{\mathrm{Fe^{3+}}\}}{\{\mathrm{Fe^{2+}}\}\cdot\{\mathrm{O_2}\}^{1/4}\cdot\{\mathrm{H^+}\}}\right) \quad (9)$$

where $\Delta G^0_{\mathrm{oxidation}}$ was the standard state Gibbs free energy calculated from ΔG^0_{f} for all products and reactants,[21] and { } represents chemical activities for all dissolved species. $\Delta G^0_{\mathrm{oxidation}}$ was adjusted to different temperatures by assuming that $\Delta H^0_{\mathrm{oxidation}}$(298 K) and $\Delta S^0_{\mathrm{oxidation}}$(298 K) remained constant over the temperature range in this study[22] (9.3−26.2 °C). Ionic strength was calculated from conductivity using a correlation developed by the USGS based on 93 samples collected from 42 active mine water treatment plants in Pennsylvania, US that ranged from 250 to 13 000 μS/cm (Charles Cravotta III, 2014; personal communication). Activity coefficients for Fe^{2+} and Fe^{3+} were calculated with the Davies equation.[23] Measured values of pH equaled p{H^+}. The activity coefficient of O_2(aq) was assumed to equal 1 for all ionic strengths. Measured values of dissolved [Fe(II)], dissolved [Fe(III)], dissolved oxygen, pH, and temperature were then used in eq 9. On the basis of reaction 2, the standard state Gibbs free energy for schwertmanite precipitation ($\Delta G^0_{\mathrm{precipitation}}$) was calculated using an equilibrium constant of log K = 18.8 (25 °C).[9] The Gibbs free energy for the precipitation of schwertmannite ($\Delta G_{\mathrm{precipitation}}$) was calculated based on {H^+}, {Fe^{3+}}, and {SO_4^{2-}}. Details of these calculations are included in the Supporting Information.

RESULTS AND DISCUSSION

Evaluation of biogeochemical kinetics in the field is challenging because the microbial community often evolves in parallel with changing geochemical conditions. A sophisticated approach to measuring low-pH Fe(II) oxidation kinetics at field scale could attempt to account for biomass concentration (as in eq 4), microbial community composition, specific activity of community members, a suite of geochemical parameters (e.g., pH, O_2, Fe(II), Fe(III), sulfate, ...) and temperature, and then integrate all these factors across the stream reach. We have, instead, attempted to simplify our kinetic analysis and incorporate the effect of many system variables into a single first-order rate constant ($k_{\mathrm{Fe(II),field}}$ or $k_{\mathrm{Fe(II),lab}}$). There are several justifications for this approach. Geochemical gradients across these sites display similar trends,[13,14,17,24,25] microbial communities evolve in similar ways[13,25,26] (primarily controlled by pH[27]), biomass concentrations remain relatively constant along the reach,[13,24,25,28] and the specific activity of many Fe(II)-oxidizing bacteria (FeOB) are similar.[29]

Geochemical gradients are established downstream of each AMD source such that dissolved oxygen increases, pH decreases, Fe(II) decreases, Fe(III) increases, and total Fe decreases.[13,14,17,24,25] The microbial ecology shifts from photoautotrophs at the emergence to chemoautotrophs further downstream.[13,25−27] Microbes more tolerant of lower pH tend to become predominant as one moves downstream. As Fe(III) minerals and organic matter (algal biomass and leaf detritus) accumulate on the stream bottom, heterotrophic Fe(III) reduction also occurs at relatively shallow depths in the stream sediments.[30] The microbial community composition does not vary much from one site to another, being comprised primarily of some combination of *Ferrovum*, *Acidithiobacillus*, *Leptospirillum*, and *Acidiphilium*.[13,25,26] Measured cell abundance or cultivatable cell numbers along AMD-impacted streams remain relatively constant (within an order of magnitude).[13,24,25,28] In the current study, we found that total PLFAs in the sediments at four of the five U.S. sites were quite similar (Table 1). On the basis of these PLFA measurements, the microbial communities were also similar (Figure S1 of the Supporting Information). Finally, the specific rates of Fe(II) oxidation for eight different FeOBs, including *Ferrovum*, *Acidithiobacilli*, and *Leptospirillum*, have been shown to vary by less than a factor of 3.[29] One the basis of these previous studies and limited microbial characterizations of the US field sites, we have evaluated both field and laboratory kinetics using a first-order model (eqs 6 and 8) where $[H^+]$ is explicitly removed from the rate equation such that we can separately evaluate the effect of pH.

Rates of low-pH Fe(II) oxidation measured at the various field sites were consistently faster than previous studies[16,31−33] (Figure 1A). For each individual set of rates (US sites, IPB sites, chemostat 1, chemostat 2), the relatively fastest rates occurred at the lowest pH values. Rates from the US field sites ranged from 1.43×10^{-6} mol Fe(II) L^{-1} s^{-1} at pH 4.05 to 9.70×10^{-6} mol Fe(II) L^{-1} s^{-1} at pH 2.73 (Table 1). Rates from the IPB field sites ranged from 13.1×10^{-7} mol Fe(II) L^{-1} s^{-1} at pH 3.13 to 67.9×10^{-7} mol Fe(II) L^{-1} s^{-1} at pH 2.36. Rates from the chemostat experiments ranged from 1.05×10^{-7} mol Fe(II) L^{-1} s^{-1} at pH 3.50 to 2.44×10^{-7} mol Fe(II) L^{-1} s^{-1} at pH 2.40 (Tables 2 and 3). Laboratory rates were slower and, on a zero-order basis, less pH-dependent as compared to field rates. Sánchez España et al.[34] measured zero-order rates of Fe(II) oxidation in laboratory experiments and also found that the corresponding field rates were almost an order of magnitude faster than the laboratory rates.

The dotted line in Figure 1A is included to show how, when considering all the rates as one set of observations, these rates are consistent with the pH-dependency proposed in eq 4. The slope of −1·pH is derived directly from the stoichiometry of reaction 1, analogous to the slope of +2·pH for the rate-dependency of the oxidative precipitation of ferrihydrite ($Fe(OH)_3$(s)):

dx.doi.org/10.1021/es501322d | Environ. Sci. Technol. 2014, 48, 9246−9254

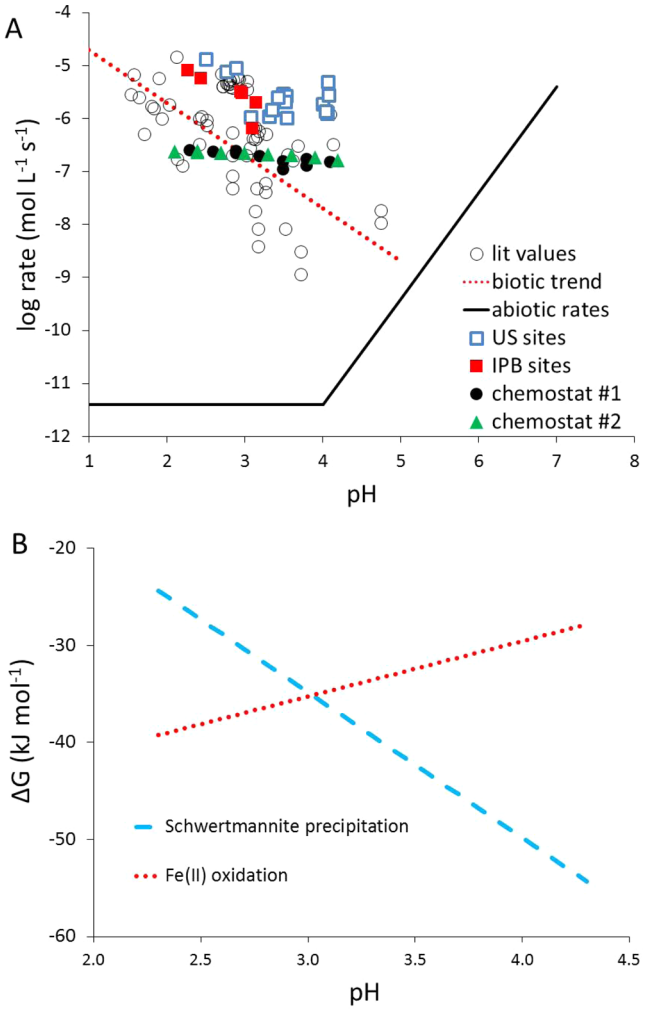

Figure 1. (A) Rates of Fe(II) oxidation reported from multiple studies and compared to the current study. Literature values compiled from Kirby and Elder Brady,[31] Sánchez-España et al.,[32] and Chen and Jiang.[33] Biotic trend included to show −1·pH dependency. Abiotic rates from Stumm and Lee.[43] (B) Gibbs free energy (ΔG) for microbial low-pH Fe(II) oxidation (reaction 1) and for schwertmannite precipitation (reaction 2). Conditions used for calculations are provided in the text and the Supporting Information.

$$Fe^{2+} + \frac{1}{4}O_2(aq) + \frac{5}{2}H_2O = 2H^+ + Fe(OH)_3(s) \quad (10)$$

shown by the rising solid line in Figure 1A. The dotted line in Figure 1B is the Gibbs free energy ($\Delta G_{oxidation}$) for Fe(II) oxidation (reaction 1) calculated using eq 9 and shows how this process becomes more favorable at lower pH. For the dotted line shown, $\{Fe^{3+}\}/\{Fe^{2+}\}$ was fixed at 10^{-2}, $\{O_2\}$ was fixed at 6.25 μM, temperature was 25 °C, and $\{H^+\}$ was the only variable. The values for the $\{Fe^{3+}\}/\{Fe^{2+}\}$ ratio and $\{O_2\}$ were selected to represent typical emergent AMD conditions. Thus, the pH-dependency of the rate of Fe(II) oxidation can be simply attributed to the amount of free energy available to the microbes catalyzing the reaction. Faster rates occur at lower pH values where $\Delta G_{oxidation}$ values are more negative.

In contrast to Fe(II) oxidation producing soluble Fe(III) (reaction 1), the precipitation of schwertmannite (reaction 2) becomes more energetically favorable as the pH increases between the pH range of 2.0−4.5 (Figure 1B). Microbes do not directly produce schwertmannite, instead a series of sequential abiotic reactions transform biogenic Fe(III) produced in reaction 1 into solid Fe(III). Assuming schwertmannite precipitation occurs according to reaction 2 and using an equilibrium constant of log K = 18.8 (25 °C),[9] $\Delta G_{precipitation}$ was calculated as a function of $\{H^+\}$ for fixed values of $\{Fe^{3+}\}$ and $\{SO_4^{2-}\}$ (per mol Fe). The dashed line in Figure 1B was calculated for $\{Fe^{3+}\}$ = 0.18 mM, $\{SO_4^{2-}\}$ = 10 mM, and 25 °C. The values for $\{Fe^{3+}\}$ and $\{SO_4^{2-}\}$ were selected to represent typical oxidized conditions for AMD that has been transported across a TIF.

First-order rate constants for Fe(II) oxidation were fastest at lower pH values (Figure 2A). Rate constants from the US field sites ranged from 0.034 min^{-1} at pH 4.07 to 0.465 min^{-1} at pH 2.73. Rate constants from the IPB field sites ranged from 0.002 min^{-1} at pH 3.10 to 0.030 min^{-1} at pH 2.27. Rate constants from the chemostat experiments ranged from 0.0020 min^{-1} at pH 3.50 with chemostat 1 (Table 2) to 0.128 min^{-1} at pH 2.40 with chemostat 2 (Table 3). Fe(II) oxidation kinetics measured in the field were 5-times slower at Brubaker Run (source of biomass for chemostat 1) as compared to Scalp Level (source of biomass for chemostat 2) (Table 1). However, differences in Fe(II) oxidation rates by the microbial communities enriched from these two sites were much smaller. Over the range of pH set-points tested, first-order rate constants for Fe(II) oxidation

Table 2. Biogeochemical Characteristics of the Laboratory Chemostat Reactor 1 (Brubaker Run) and Corresponding Fe(II) Oxidation Kinetics[a]

reactor pH	reactor O_2(aq) (mg L^{-1})	influent dissolved Fe(II) (mg L^{-1})	reactor biomass (×10^7 cell mL^{-1})	$R_{Fe(II),lab}$(×10^7 mol L^{-1} s^{-1})	$k_{Fe(II),lab}$ (min^{-1})	n
2.90	7.2 ± 1.1	346 ± 7.7	0.63	2.41	0.146	4
2.60	5.2 ± 0.3	313 ± 15	1.9	2.31	0.0226	3
2.30	5.9 ± 1.3	311 ± 15	0.94	2.43	0.0469	5
2.60	8.6	304	0.77	n.d.	n.d.	1
2.90	6.1 ± 0.3	299 ± 21	2.3	2.19	0.0212	2
3.20	6.4 ± 0.6	305 ± 5.5	1.1	1.92	0.0087	8
3.50	4.8 ± 0.3	306 ± 3.5	0.47	1.53	0.0042	3
3.80	4.1 ± 0.3	300 ± 2.5	1.2	1.65	0.0055	5
4.10	5.4 ± 2.1	301 ± 4.4	0.92	1.49	0.0041	5
3.80	3.9 ± 0.7	304 ± 0.0	0.48	1.27	0.0028	5
3.50	3.1 ± 0.7	303 ± 2.9	0.44	1.05	0.0020	6

[a]Values represent mean ± one standard deviation for n sampling points during pseudo-steady-state conditions. n.d. = not determined based on only one pseudo-steady-state time point.

dx.doi.org/10.1021/es501322d | Environ. Sci. Technol. 2014, 48, 9246−9254

Table 3. Biogeochemical Characteristics of the Laboratory Chemostat Reactor 2 (Scalp Level) and Corresponding Fe(II) Oxidation Kinetics[a]

reactor pH	reactor O_2(aq) (mg L^{-1})	influent dissolved Fe(II) (mg L^{-1})	reactor biomass ($\times 10^7$ cell mL^{-1})	$R_{Fe(II),lab}$ ($\times 10^7$ mol L^{-1} s^{-1})	$k_{Fe(II),lab}$ (min^{-1})	n
2.70	6.9 ± 0.4	314 ± 11.9	1.1	2.22	0.0161	5
2.40	7.5 ± 0.3	300 ± 12.0	1.8	2.44	0.128	2
2.10	7.8 ± 0.4	297 ± 12.5	0.94	2.36	0.0582	7
2.40	7.0 ± 0.1	295 ± 4.2	3.4	2.33	0.0556	2
2.70	7.9 ± 0.4	300 ± 4.2	4.9	2.22	0.0228	5
3.00	8.2 ± 0.3	297 ± 2.3	1.6	2.21	0.0245	4
3.30	8.1 ± 0.4	309 ± 9.4	1.4	2.08	0.0119	3
3.60	7.5 ± 0.3	292 ± 6.4	1.5	2.01	0.0135	6
3.90	7.7 ± 0.7	342 ± 11.7	2.3	1.86	0.00529	3
4.20	7.7 ± 0.3	299 ± 8.1	2.5	1.63	0.00536	5

[a]Values represent mean ± one standard deviation for n sampling points during pseudo-steady-state conditions.

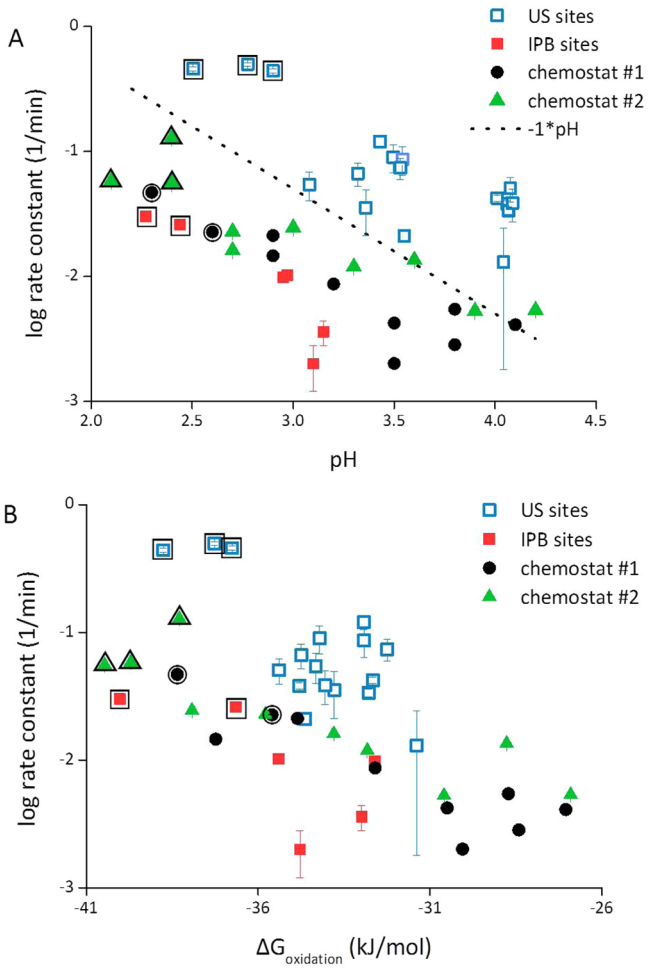

Figure 2. (A) First-order rate constants for Fe(II) oxidation versus pH. pH values for the field series were taken from the AMD emergence. pH values for the chemostat series were taken from the reactor set-point. The dotted line is included to show −1·pH dependency. Enlarged borders around select data points correspond to the same data in both panels A and B. Standard error shown with error bars, otherwise smaller than symbol. (B) First-order rate constants for Fe(II) oxidation versus Gibbs free energy for microbial low-pH Fe(II) oxidation ($\Delta G_{oxidation}$). $\Delta G_{oxidation}$ values were calculated based on site- and condition-specific geochemical measurements.

were 1.1-times slower in chemostat 1 as compared to chemostat 2. The convergence of these rates could have been caused by identical conditions used in the laboratory tests versus different physical and hydrodynamic conditions encountered at each field site. The −1·pH dotted line in Figure 2A is included only for visual reference.

The rate of microbial respiration has been shown to be dependent on the amount of free energy available to the microbes.[35,36] Jin and Bethke[35,36] proposed a rate law for microbial respiration that includes a thermodynamic factor (F_T) similar to a saturation index (Q/K_{sp}) term commonly used to adjust the kinetics of mineral precipitation/dissolution.[37] Their rate law was derived on the basis of chemiosmotic theory and accounts for forward and reverse fluxes through the electron transport chain and the energy required for ATP synthesis. Bethke et al.[38] validated this rate law by measuring and modeling the populations of sulfate reducers, iron reducers, and methanogens in long-term, energy-limited laboratory experiments. We hypothesized that the rate of low-pH Fe(II) oxidation in both the field and in our laboratory reactors were similarly controlled by free energy, in this case $\Delta G_{oxidation}$ as calculated by eq 9.

First-order rate constants for Fe(II) oxidation were dependent on the $\Delta G_{oxidation}$ calculated for each specific site and each specific chemostatic condition (Figure 2B). For the field sites, $\Delta G_{oxidation}$ was calculated based on the geochemical conditions (dissolved [Fe(II)], dissolved [Fe(III)], [O_2(aq)], pH, temperature, and conductivity) at the emergent source of AMD. For the chemostat experiments, $\Delta G_{oxidation}$ was calculated based on the geochemical conditions in the influent feed tank (dissolved [Fe(II)], dissolved [Fe(III)]) and in the reactor vessel ([O_2(aq)], pH, temperature, and conductivity). These geochemical conditions essentially represented the greatest potential energy for microbes to gain from oxidizing Fe(II). In contrast to the thermodynamic calculations presented in Figure 1B, only measured values were used for the data shown in Figure 2B.

Statistical analyses were employed to examine the significance of the relationships between the first-order rate constant versus pH (Figure 2A) and the first-order rate constant versus $\Delta G_{oxidation}$ (Figure 2B) for each series (US sites, IPB sites, chemostat 1, chemostat 2), and the difference of the regression slopes of each series by pairwise comparisons. t tests demonstrated that all regression equations for log rate constant-vs-pH described the data at a 95% significance level (Table S1 of the Supporting Information). All regression equations for log rate constant-vs-$\Delta G_{oxidation}$, except for the IPB sites, also described the data at a 95% significance level. Pair-

dx.doi.org/10.1021/es501322d | Environ. Sci. Technol. 2014, 48, 9246−9254

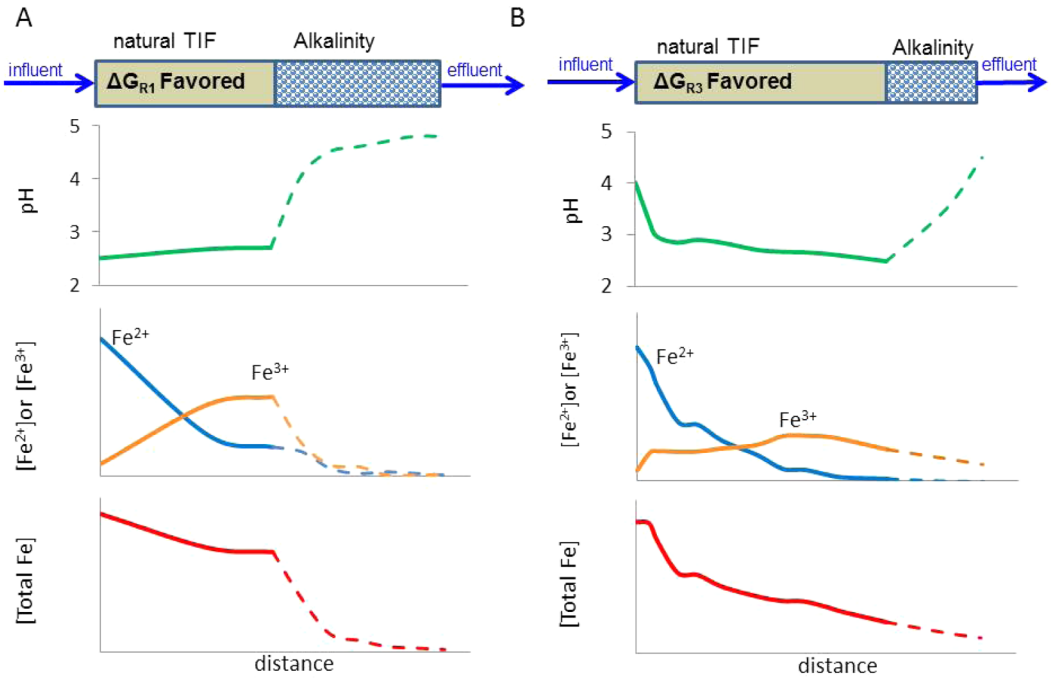

Figure 3. Conceptual schematics of passive treatment systems for anoxic, acidic, Fe(II)-rich acid mine drainage (AMD). An "engineered" terraced iron formation (TIF) would include a natural TIF followed by an alkaline channel. (A) Configuration for an extremely acidic discharge where the oxidation of Fe(II) to soluble Fe(III) (reaction 1) would be thermodynamically favored. Solid lines are observations from Scalp Level, dashed lines are conceptual predictions. (B) Configuration for a moderately acidic discharge where the oxidation of Fe(II) to insoluble Fe(III) (reaction 3) would be thermodynamically favored. Solid lines are observations from Upper Red Eyes.

wise comparisons of all the log rate constant-vs-pH regressions demonstrated that all slope coefficients were not significantly different at a 95% significance level (Table S2 of the Supporting Information). Similarly, all slope coefficients from the log rate constant-vs-$\Delta G_{oxidation}$ regressions were not significantly different.

The fastest rates of Fe(II) oxidation occurred at the lowest pH values and all corresponded with the most negative values of $\Delta G_{oxidation}$ (Figure 2). Enlarged symbols in Figure 2A and 2B are used to highlight the same data points in both panels for the four sets of rates. Less negative values of $\Delta G_{oxidation}$ for the chemostat experiments were caused by the partial oxidation of Fe(II) in the influent feed tank solutions. The fastest rates of Fe(II) oxidation also occurred under conditions where the production of soluble Fe(III) (reaction 1) was predominant versus the oxidative precipitation of schwertmannite (reaction 3). An increase in pH (i.e., consumption of H^+) is consistent with reaction 1 as compared to reaction 3. In the field, this was evident by a pH increase across the TIFs where the fastest rates of Fe(II) oxidation were measured (Table S3 of the Supporting Information). In the chemostat experiments, this was evident by titrant addition of acid to maintain the preset pH (Table S4 of the Supporting Information). The slower rates of Fe(II) oxidation occurred at higher pH values where schwertmannite precipitation became predominant as compared to the production of soluble Fe(III). In the chemostat experiments, this was evident by titrant addition of base to maintain the preset pH. In the field, this was evident by a pH decrease across the TIF and a decrease in dissolved Fe, plus the visual evidence of ocherous sediments deposited across the TIFs.

While $\Delta G_{oxidation}$ will become more negative as pH decreases (Figure 1B), we note that the correlation between field Fe(II) oxidation kinetics and pH will likely be valid over a limited pH range. In our study, pH values varied from 2.1 to 4.2 and span the great majority of pH conditions found in AMD systems worldwide.[39] We contend that the correlation between field Fe(II) oxidation kinetics and pH would likely apply from pH 2.0 to 5.0 for the following reasons. Low pH (<2.0) can be inhibitory to the growth and activity of FeOB, while precipitation of Fe(III) solids at higher pH (>4.0) can also inhibit FeOB.[40] We suspect that at extremely low pH values (<1.0), microbial diversity would be substantially less as compared to pH 2.1 to 4.2 because the optimum pH for growth of most acidophilic Fe(II) oxidizers is between pH 1.0 to 3.0.[41,42] Because biomass concentrations are incorporated into the first-order rate constant in our kinetic model (eq 8), slower rates would be measured at sites with lower biomass despite the high $\Delta G_{oxidation}$ available to the microbes. Because abiotic Fe(II) oxidation will become substantial above pH 5.0,[43,44] Fe(II) oxidation kinetics could increase even though $\Delta G_{oxidation}$ would decrease according to eq 9. Biomass concentrations remained relatively constant in the laboratory chemostat experiments (0.44×10^7 to 2.3×10^7 cell mL^{-1} in chemostat 1, Table 2; 0.94×10^7 to 4.9×10^7 cell mL^{-1} in chemostat 2, Table 3) supporting our approach to incorporate biomass into the first-order rate constant. On the basis of pyrosequencing of the biofilm samples collected from chemostat 1, the microbial communities remained relatively similar over the whole range of pH set-points (Figure S2 of the Supporting Information), also supporting our approach to incorporate the microbial community into the first-order rate constant.

■ ENVIRONMENTAL IMPLICATIONS

Microbial low-pH Fe(II) oxidation could be readily incorporated into passive treatment systems by enhancing natural TIFs

dx.doi.org/10.1021/es501322d | Environ. Sci. Technol. 2014, 48, 9246−9254

to create so-called engineered TIFs (Figure 3). Thermodynamic controls on the rates of low-pH Fe(II) oxidation and the predominant production of soluble Fe(III) versus insoluble Fe(III) solids would have important implications on how this process can best be exploited for AMD treatment. Regional geology and local hydrogeochemistry control the flow and geochemical conditions of the AMD that must be treated. Extremely acidic waters could be manipulated to promote the fastest rates of Fe(II) oxidation. The trade-off for exploiting faster rates at lower pH values is that less dissolved Fe will be removed. From field studies we have found that "oxidation channels" built from alkaline materials such as concrete or limestone remove significant amounts of dissolved Fe but with little change in pH.[17] Engineered TIFs, therefore, could be designed to use natural TIFs followed with an alkaline channel. The alkalinity in this channel would not be sized to neutralize the influent acidity but instead to counterbalance the acidity generated by Fe(III) precipitation within the channel. The hydrodynamics of the channel would be similar to the shallow sheet flow commonly seen across natural TIFs. The natural TIF would provide the microbial seed to colonize the downstream alkaline channel.

Conceptually, the relative sizes of the natural TIF and alkaline channel would be determined based on the thermodynamic favorability of the production of soluble Fe(III) (reaction 1) versus the production of schwertmannite (reaction 3). The solubility of schwertmannite (K_{sp}) and $\Delta G_{precipitation}$, and their noted uncertainties, will factor directly into the thermodynamic favorability of reaction 1 versus reaction 3. If an emergent AMD source was extremely acidic such that rapid production of soluble Fe(III) was favored, an equal-sized alkaline channel would be helpful to raise the pH and promote Fe(III) precipitation (Figure 3A). If an emergent AMD source had a pH that favored the oxidative precipitation of Fe(III), a relatively smaller sized alkaline channel would be used to help promote the removal of correspondingly lower concentrations of Fe(III). The geochemical trends shown as solid lines for the natural TIF portions in Figure 3 are from actual sites in the US; Figure 3A from Scalp Level, and Figure 3B from Upper Red Eyes. The geochemical trends shown as dashed lines for the alkaline channel portions are conceptual predictions.

Similarly, microbial low-pH Fe(II) oxidation could be incorporated into an active treatment system. In a pilot-scale three-chamber reactor system, pH was manipulated to optimize both Fe(II) oxidation and Fe(III) precipitation.[4] The first chamber was a suspended-growth bioreactor, the second chamber was used for pH adjustment to precipitate Fe(III), and the third chamber was an attached-growth bioreactor used to oxidize any remaining Fe(II). The fastest rate of Fe(II) oxidation occurred in the first chamber where the influent was pH 2.1 and the effluent increased to pH 2.3. The pH in the second reactor was adjusted with NaOH to pH 3.5 to rapidly precipitate schwertmannite from solution. A slower rate of Fe(II) oxidation occurred in the third chamber, where the influent was pH 3.5 and the effluent decreased to pH 3.3. In this example, the differing rates of Fe(II) oxidation as a function of pH were consistent with all of our field and laboratory studies—faster rates at lower pH where Fe(III) is more soluble.

AMD is a worldwide problem affecting important freshwater resources. Some of the areas most severely impacted by AMD are in arid and semiarid climates where water availability is an even greater issue. Low-pH Fe(II) oxidation can be incorporated into active or passive treatment systems for more cost-effective AMD treatment options. The treated water should be considered as an economic and natural resource for beneficial reuse. The geochemical conditions of the emergent AMD set thermodynamic conditions that influence both the rate and predominant products of Fe(II) oxidation. This simple linkage between thermodynamics and microbial kinetics should be broadly applicable to many other biogeochemical systems.

■ ASSOCIATED CONTENT

Supporting Information

Details of laboratory and field methods, details of thermodynamic calculations, regression equations, statistical comparison, change in pH across sites, titrant addition rates, and microbial characterizations. This material is available free of charge via the Internet at http://pubs.acs.org.

■ AUTHOR INFORMATION

Corresponding Author

*E-mail: wdb3@psu.edu.

Notes

The authors declare no competing financial interest.

■ ACKNOWLEDGMENTS

This work was partially supported by the US Office of Surface Mining Reclamation and Enforcement under Cooperative Agreement S11AC20005, by the Appalachian Research Initiative for Environmental Science (ARIES), and by the Spanish Ministry of Science and Innovation (project CGL2009-09070). ARIES is an industrial affiliates program at Virginia Tech, supported by members that include companies in the energy sector. The opinions and recommendations expressed herein are solely those of the authors and do not imply any endorsement by ARIES. This manuscript benefitted from comments and suggestions by three anonymous reviewers.

■ REFERENCES

(1) Trout Unlimited. *The West Branch Susquehanna Recovery Benchmark Project. A Watershed in Recovery*; Trout Unlimited: Lock Haven, PA, 2011; pp 1−12.

(2) Cravotta, C. A., III Dissolved metals and associated constituents in abandoned coal-mine discharges, Pennsylvania, USA. Part 1: Constituent quantities and correlations. *Appl. Geochem.* **2008**, *23*, 166−202.

(3) DeSa, T.; Brown, J.; Burgos, W. Laboratory and field-scale evaluation of low-pH Fe(II) oxidation at Hughes Borehole, Portage, Pennsylvania. *Mine Water Environ.* **2010**, *29* (4), 239−247.

(4) Hedrich, S.; Johnson, D. B. A modular continuous flow reactor system for the selective bio-oxidation of iron and precipitation of schwertmannite from mine-impacted waters. *Bioresour. Technol.* **2012**, *106*, 44−49.

(5) Janneck, E.; Arnold, I.; Koch, T.; Meyer, J.; Burghardt, D.; Ehinger, S. Microbial synthesis of schwertmannite from lignite mine water and its utilization for removal of arsenic from mine waters and for production of iron pigments. In *Proceedings of the International Mine Water Association*, Sydney, Nova Scotia, 2010; Wolkersdorfer, C.; Freund, A., Eds.; International Mine Water Association: Sydney, Nova Scotia, Canada, 2010; pp 131−134.

(6) Singer, P. C.; Stumm, W. Acidic mine drainage. Rate determining step. *Science* **1970**, *167*, 121−123.

(7) Nordstrom, D. *The Rate of Ferrous Iron Oxidation in a Stream Receiving Acid Mine Effluent*, Selected Papers in the Hydrologic Sciences, U.S. Geological Survey Water-Supply Paper 2270; U.S. Geological Survey: Reston, VA, 1985; pp 113−119.

(8) Bigham, J. M.; Schwertmann, U.; Traina, S. J.; Winland, R. L.; Wolf, M. Schwertmannite and the chemical modeling of iron in acid sulfate waters. *Geochim. Cosmochim. Acta* **1996**, *60* (12), 2111−2121.
(9) Sánchez-España, J.; Yusta, I.; Diez-Ercilla, M. Schwertmannite and hydrobasaluminite: A re-evaluation of their solubility and control on the iron and aluminium concentration in acidic pit lakes. *Appl. Geochem.* **2011**, *26* (9−10), 1752−1774.
(10) Caraballo, M. A.; Rimstidt, J. D.; Macías, F.; Nieto, J. M.; Hochella, M. F., Jr Metastability, nanocrystallinity and pseudo-solid solution effects on the understanding of schwertmannite solubility. *Chem. Geol.* **2013**, *360−361*, 22−31.
(11) Kawano, M.; Tomita, K. Geochemical modeling of bacterially induced mineralization of schwertmannite and jarosite in sulfuric acid spring water. *Am. Mineral.* **2001**, *86*, 1156−1165.
(12) Yu, J. Y.; Heo, B.; Choi, I. K.; Cho, J. P.; Chang, H. W. Apparent solubilities of schwertmannite and ferrihydrite in natural stream waters polluted by mine drainage. *Geochim. Cosmochim. Acta* **1999**, *63*, 3407−3416.
(13) Brown, J. F.; Jones, D. S.; Mills, D. B.; Macalady, J. L.; Burgos, W. D. Application of a depositional facies model to an acid mine drainage site. *Appl. Environ. Microbiol.* **2010**, *77*, 545−554.
(14) Sánchez España, J.; Santofimia Pastor, E.; López Pamo, E. Iron terraces in acid mine drainage systems: A discussion about the organic and inorganic factors involved in their formation through observations from the Tintillo acidic river (Riotinto mine, Huelva, Spain). *Geosphere* **2007**, *3*, 133−151.
(15) Pesic, B.; Oliver, D. J.; Wichlacz, P. An electrochemical method of measuring the oxidation rate of ferrous to ferric iron with oxygen in the presence of Thiobacillus ferrooxidans. *Biotechnol. Bioeng.* **1989**, *33* (4), 428−439.
(16) Kirby, C. S.; Thomas, H. M.; Southam, G.; Donald, R. Relative contributions of abiotic and biological factors in Fe(II) oxidation in mine drainage. *Appl. Geochem.* **1999**, *14* (4), 511−530.
(17) Larson, L. N.; Sánchez-España, J.; Burgos, W. Rates of low-pH biological Fe(II) oxidation in the Appalachian Bituminous Coal Basin and the Iberian Pyrite Belt. *Appl. Geochem.* **2014**, DOI: 10.1016/j.apgeochem.2014.05.012.
(18) Stookey, L. L. Ferrozine—A new spectrophotometric reagent for iron. *Anal. Chem.* **1970**, *42* (7), 779−781.
(19) Kaley, B. Low-pH Fe(II) oxidation using a bioreactor for the treatment of acid mine drainage. MS Thesis, The Pennsylvania State University, University Park, PA, 2013.
(20) Leistel, J. M.; Marcoux, E.; Thiéblemont, D.; Quesada, C.; Sánchez, A.; Almodóvar, G. R.; Pascual, E.; Sáez, R. The volcanic-hosted massive sulphide deposits of the Iberian Pyrite Belt review and preface to the thematic issue. *Miner. Deposita* **1997**, *33* (1−2), 2−30.
(21) Stumm, W.; Morgan, J. J. *Aquatic Chemistry: Chemical Equilibria and Rates in Natural Waters*, 3rd ed.; John Wiley and Sons: New York, 1996.
(22) Anderson, G. M. *Thermodynamics of Natural Systems*; Cambridge University Press: New York, 2008.
(23) Bethke, C. M. *Geochemical and Biogeochemical Reaction Modeling*, 2nd ed.; Cambridge University Press: New York, 2008.
(24) Walton, K. C.; Johnson, D. B. Microbiological and chemical characteristics of an acidic stream draining a disused copper mine. *Environ. Pollut.* **1992**, *76*, 169−175.
(25) Rowe, O. F.; Sánchez España, J.; Hallberg, K. B.; Johnson, D. B. Microbial communities and geochemical dynamics in an extremely acidic, metal-rich stream at an abandoned sulfide mine (Huelva, Spain) underpinned by two functional primary production systems. *Environ. Microbiol.* **2007**, *9* (7), 1761−1771.
(26) González-Toril, E.; Aguilera, A.; Souza-Egipsy, V.; López Pamo, E.; Sánchez España, J.; Amils, R. Geomicrobiology of La Zarza-Perrunal acid mine effluent (Iberian Pyritic Belt, Spain). *Appl. Environ. Microbiol.* **2011**, *77* (8), 2685−2694.
(27) Kuang, J.-L.; Huang, L.-N.; Chen, L.-X.; Hua, Z.-S.; Li, S.-J.; Hu, M.; Li, J.-T.; Shu, W.-S. Contemporary environmental variation determines microbial diversity patterns in acid mine drainage. *ISME J.* **2013**, *7*, 1038−1050.
(28) McGinness, S.; Johnson, D. B. Seasonal variations in the microbiology and chemistry of an acid mine drainage stream. *Sci. Total Environ.* **1993**, *132*, 27−41.
(29) Johnson, D. B.; Kanao, T.; Hedrich, S. Redox transformations of iron at extremely low pH: Fundamental and applied aspects. *Front. Microbiol.* **2012**, *3*, 96 DOI: 10.3389/fmicb.2012.00096.
(30) Coupland, K.; Johnson, D. B. Evidence that the potential for dissimilatory ferric iron reduction is widespread among acidophilic heterotrophic bacteria. *FEMS Microbiol. Lett.* **2008**, *279*, 30−35.
(31) Kirby, C. S.; Elder-Brady, J. A. Field determination of Fe^{2+} oxidation rates in acid mine drainage using a continuously-stirred tank reactor. *Appl. Geochem.* **1998**, *13* (4), 509−520.
(32) Sánchez España, J.; López Pamo, E.; Santofimia Pastor, E. The oxidation of ferrous iron in acidic mine effluents from the Iberian Pyrite Belt (Odiel Basin, Huelva, Spain): Field and laboratory rates. *J. Geochem. Explor.* **2007**, *92* (2−3), 120−132.
(33) Chen, C.-J.; Jiang, W.-T. Influence of waterfall aeration and seasonal temperature variation on the iron and arsenic attenuation rates in an acid mine drainage system. *Appl. Geochem.* **2012**, *27* (10), 1966−1978.
(34) Sánchez España, J.; López Pamo, E.; Santofimia Pastor, E. The oxidation of ferrous iron in acidic mine effluents from the Iberian Pyrite Belt (Odiel Basin, Huelva, Spain): Field and laboratory rates. *J. Geochem. Explor.* **2007**, *92*, 120−132, DOI: 10.1016/j.gexplo.2006.08.010.
(35) Jin, Q.; Bethke, C. M. A new rate law describing microbial respiration. *Appl. Environ. Microbiol.* **2002**, *69*, 2340−2348, DOI: 10.1128/AEM.69.4.2340-2348.2003.
(36) Jin, Q.; Bethke, C. M. Predicting the rate of microbial respiration in geochemical environments. *Geochim. Cosmochim. Acta* **2002**, *69*, 1133−1143, DOI: 10.1016/j.gca.2004.08.010.
(37) Lasaga, A. C. Rate Laws of Chemical Reactions. In *Kinetics of Geochemical Processes*; Lasaga, A. C., Kirkpatrick, R. J., Eds.; Mineralogical Society of America, BookCrafters Inc., Chelsea, MI, 1981; pp 1−68.
(38) Bethke, C. M.; Sanford, R. A.; Kirk, M. F.; Jin, Q.; Flynn, T. M. The thermodynamic ladder in geomicrobiology. *Am. J. Sci.* **2011**, *311*, 183−210.
(39) Nordstrom, D. K.; Alpers, C. N. Geochemistry of acid mine waters. In *The Environmental Geochemistry of Mineral Deposits, Part A. Processes, Techniques, and Health Issues*; Plumlee, G. S., Logsdon, M. J., Eds.; Society of Economic Geologists: Littleton, CO, 1999; Vol. *6A*, pp 133−156.
(40) Meruane, G.; Vargas, T. Bacterial oxidation of ferrous iron by *Acidithiobacillus ferrooxidans* in the pH range 2.5−7.0. *Hydrometallurgy* **2003**, *71*, 149−158.
(41) Baker-Austin, C.; Dopson, M. Life in acid: pH homeostasis in acidophiles. *Trends Microbiol.* **2007**, *15* (4), 165−171.
(42) Johnson, D. B. Biodiversity and ecology of acidophilic microorganisms. *FEMS Microbiol. Ecol.* **1998**, *27*, 307−317.
(43) Stumm, W.; Lee, G. F. Oxygenation of ferrous iron. *Ind. Eng. Chem.* **1961**, *53*, 143−146.
(44) Wehrli, B. Redox reactions of metal ions at mineral surfaces. In *Aquatic Chemical Kinetics*; John Wiley & Sons: New York, 1990.
(45) Kirby, C. S.; Cravotta, C. A. Net alkalinity and net acidity 1: Theoretical considerations. *Appl. Geochem.* **2005**, *20*, 1920−1940.